An Open-Source OpenSim Oculomotor Model for Kinematics and Dynamics Simulation

Konstantinos Filip, Dimitar Stanev[1], and Konstantinos Moustakas

August 22, 2018

[1]Electrical and Computer Engineering Department, University of Patras, Greece; Corresponding author: stanev@ece.upatras.gr

Abstract

Physics-based modeling and dynamic simulation of human eye movements has significant implications for improving our understanding of the oculomotor system and treating various visuomotor disorders. We introduce an open-source biomechanical model of the human eye that can be used for kinematics and dynamics analysis. This model is based on the passive pulley hypothesis, constructed based on the data reported in literature regarding physiological measurements of the human eye and made publicly available[1]. The model is implemented in `OpenSim`, which is an open-source framework for modeling and simulation of musculoskeletal systems. The model incorporates an eye globe, orbital suspension tissues and six extraocular muscles. The excitation and activation patterns for a variety of targets can be calculated using the proposed closed-loop fixation controller that drives the model to perform saccadic movements in a forward dynamics manner. The controller minimizes the error between the desired saccadic trajectory and the predicted movement. Consequently, this model enables the investigation muscle activation patterns during static fixation and analyze the dynamics of eye movements.

---

[1]SimTK project: `https://simtk.org/projects/eye`

Introduction

Rapid and accurate eye movements are of great importance for natural vision and thus studying human eye movement can improve our understanding of the oculomotor system and treating various visuo-motor disorders Lee and Terzopoulos (2006); Wei et al. (2010). Over the past decades, biomechanics simulation has provided the means to analyze different human movements Delp et al. (2007). The same principles can be used to analyze visual tasks by modeling the musculoskeletal properties of the oculomotor system. Consequently, this model can be used to investigate muscle activation patterns during static fixation, analyze the dynamics of various eye movements, calculate metabolic costs and simulate eye disorders, such as different forms of strabismus Wong (2004). Furthermore, it can be easily integrated with available full body models in order to analyze the relation between the vestibular and oculomotor systems.

Eye movements are a generated from the coordinated activation of the six Extraocular Muscles (EOMs). Clinical trials have provided a profound knowledge on the properties of the EOMs and their line of action on the eye globe Robinson et al. (1969) and the resistive tension of the surrounding tissues Collins et al. (1981); Iskander et al. (2018). Various computational models of the extraocular muscles and orbital mechanics have been proposed, which provide insight for oculomotor biomechanics, control of eye movement Bach-y Rita et al. (1971) and binocular misalignment. These models focus on the realism of muscle behavior and they were based on the viscoelastic properties and physiological data EOMs.

The first 3D biomechanical model was developed by Robinson (1964); Robinson and Fuchs (1969), who simplified the formulation by only considering the elasticity of the EOMs ignoring their dynamics. The model incorporates anatomically realistic muscle paths and empirical innervation-length-tension relationships. In order to study the neural control of rapid saccadic movements, models using anatomical and mechanical properties of EOMs have been developed by accounting for the nonlinear muscle dynamics Thelen et al. (2003); Millard et al. (2013). Such models, having the advantage of supporting dynamics simulation, are used in conjunction with brain level controllers Angelaki and Hess (2004); James et al. (2018).

Methods

Eye Modeling

The eye model consists of the eye globe, three pairs of EOMs and the connective passive tissues. The size of an emmetropic human adult eye is approximately 0.0242m (transverse, horizontal), 0.0237m (sagittal, vertical), $0.022 - 0.0248$m (axial, anteroposterior) with no significant difference between sexes and age groups. In the transverse diameter, the eye may vary from 0.021m to 0.027m, thus it can be approximated by a solid sphere of radius $r = 0.012$m. The weight of an average human eye is $m = 0.0075$kg and the moment of inertia can be calculated assuming a spherical homogeneous and isotropic model $I = 2/5mr^2$. The eye has three rotational Degrees of Freedom (DoFs), namely incyclotosion-excyclotosion (x-axis), adduction-abduction (y-axis) and supraduction-infraduction (z-axis).

Muscle Modeling

The six EOMs, including four rectus muscles and two oblique muscles, are controlled by the cranial nerves so as to track a visual target and to stabilize the image of the object of interest on the retina. The Lateral Rectus (LR) and Medial Rectus (MR) muscles form an agonist/antagonist pair that produce horizontal eye movements. The Superior Rectus (SR) and Inferior Rectus (IR) muscles form the vertical agonist/antagonist pair, which mainly controls vertical eye movement and also affects rotation about the

line of sight (secondary action) and the horizontal plane (tertiary action). The Superior Oblique (SO) muscle passes through the cartilaginous trochlea attached to the orbital wall, which reflects the SO path by 51°. The Inferior Oblique (IO) muscle originates from the orbital wall anteroinferior to the globe center and inserts on the sclera posterior to the globe equator. The primary actions of SO and IO cause rotation of the globe around the visual axis, but also affect vertical (secondary action) and horizontal (tertiary action) movements.

The model relies on the passive pulley assumption, which states that the pulleys have fixed to the orbit pulley points Clark et al. (1977); Miller (2007). Table 1 shows the positions of the origin, insertion and pulleys for the EOMs, defined in the local body coordinates of the eye globe. The data are based on physiological measurements Iskander et al. (2018), with some minor modification so as to prevent unrealistic muscle-surface penetration. Since no position was documented for the origin of the SO, a point close to the origins of the rectus muscles was chosen to match the fiber length in the primary position of the SO muscle.

Table 1: Muscle path points for the six EOMs defined in the local frame of the eye globe (dimensions are given in meters).

Muscle	Origin			Pulley			Insertion		
	Ox	*Oy*	*Oz*	*Px*	*Py*	*Pz*	*Ix*	*Iy*	*Iz*
LR	-0.034	0.0006	-0.013	-0.0102	0.0003	0.012	0.0065	0	0.0101
MR	-0.030	0.0006	-0.017	-0.0053	0.00014	-0.0146	0.0088	0	-0.0096
SR	-0.0317	0.0036	-0.016	-0.0092	0.012	-0.002	0.0076	0.0104	0
IR	-0.0317	-0.0024	-0.016	-0.0042	-0.0128	-0.0042	0.00805	-0.0102	0
SO	0.0082	0.0122	-0.0152	-0.030834	0.001145	-0.01644	0.0044	0.011	0.0029
IO	0.0113	-0.0154	-0.0111	-0.00718	-0.0135	0	-0.008	0	0.009

The Millard muscle model Millard et al. (2013) has been adopted for the modeling of the EOMs, permitting parameterization of the characteristic curves according to the experimental measured data. The muscles were modeled using the rigid tendon assumption that ignores the elasticity of the tendon. This means that the series element of the muscle model is not included (the tendon length l^T is equal to the tendon slack length l_s^T). EOMs are considered parallel-fibered muscles, so the pennation angle is zero ($\alpha = 0$). The values for the maximum isometric force f_o^M, optimal fiber length l_o^M and tendon length l^T are presented in Table 2.

Table 2: Millard muscle parameters for the EOMs.

Muscle	Maximum Isometric Force (N)	Optimal Fiber Length (m)	Tendon Slack Length (m)	Maximum Contraction Velocity (m / s)
LR	1.4710	0.04898	0.0084	3.8483
MR	1.5740	0.04084	0.0038	4.6155
SR	1.1768	0.04487	0.0054	4.2009
IR	1.4269	0.04549	0.0048	4.1437
SO	0.6031	0.03956	0.0265	4.7648
IO	0.5590	0.04110	0.0015	4.5863

The active Force-Length (F-L) and Passive-Force-Length (F-PE) characteristic curves of the EOMs differ significantly from those of a skeletal muscle. As shown in Figure 1, we can fine-tune the curve parameters so as to fit the experimental data available for the LR muscle. The values for the active F-L

Table 3: Parameters of the active F-L characteristic curve for the EOMs.

Parameter	Value
min norm active fiber length	0.55
transition norm fiver length	0.7
max norm active fiver length	1.8
shallow ascending slope	2.4
minimum value	0.0

Table 4: Parameters of the F-PE characteristic curve for the EOMs.

Parameter	Value
strain at zero force	-0.18
strain at one norm force	0.4

and F-PE characteristic curves are summarized in Tables 3 and 4, respectively. We safely assume that the parameters of the characteristic curves for the other EOMs are the same.
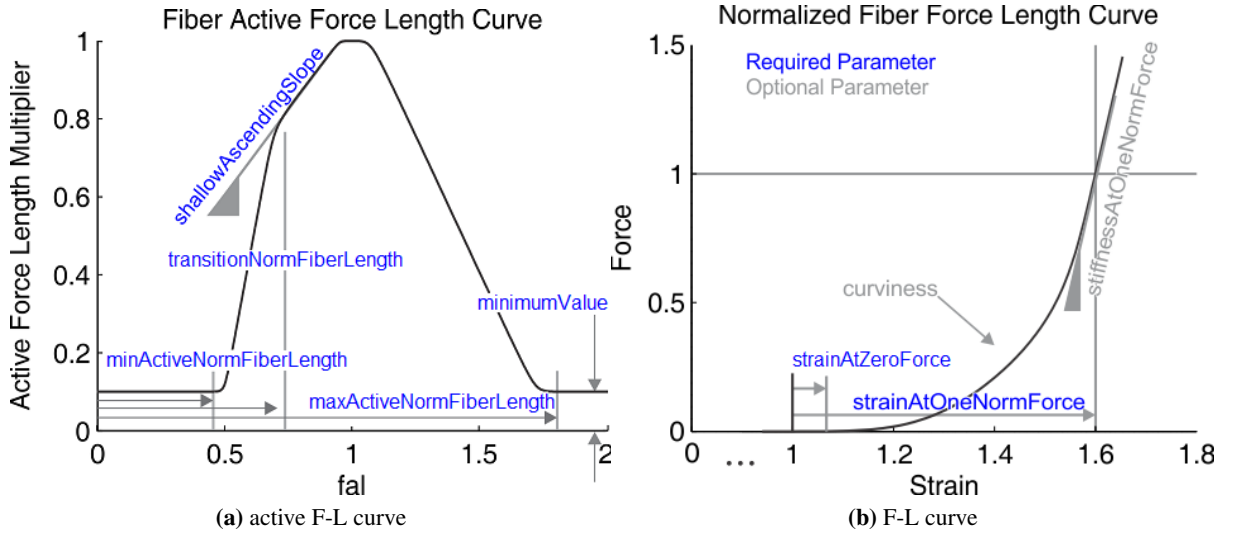

(a) active F-L curve

(b) F-L curve

Figure 1: The active F-L and F-PE curve definition for the Millard muscle model as implemented in `OpenSim`.

EOMs have a higher fraction of fast twitch fibers and thus different Force-Velocity (F-V) behavior, due to different structures compared to skeletal muscles. Despite that, the default Millard F-V curve was used for the six EOMs, since the behavior of the selected muscle model depends heavily on the maximum contraction velocity v^{max}. The maximum muscle contraction velocity is tuned so as to match the peak velocity of saccadic eye movement $\omega^{\mathrm{max}} = 15.7\mathrm{rad/s}$ ($900°/\mathrm{s}$). Following this definition, the maximum muscle contraction velocity is given in optimal fiber length per seconds and it is thus different for each EOMs, as their optimal fiber length is different ($v^{\mathrm{max}} = \omega^{\mathrm{max}} r/l_o^M$). Furthermore, since the optic nerve is much shorter that the average muscle nerve, activation and deactivation delays ($\tau_a = \tau_d = 5\mathrm{ms}$) are smaller. Finally, two separate wrapping spheres for the rectus muscles and the oblique muscles were created, to avoid abnormal changes on the F-L curve as the eye rotates.

Passive Connective Tissues

The passive connective tissues of the orbit apply a restoring force, which brings the eye back to the central position when the net force from the EOMs is zero. These tissues include all non-muscular suspensory tissues, such as Tenon's capsule, the optic nerve, the fat pad and the conjunctiva. The force-displacement elasticity force can be represented as

$$\boldsymbol{f}_t = -k_p \boldsymbol{q} - k_c \boldsymbol{q}^3 - k_v \dot{\boldsymbol{q}} \tag{1}$$

where, $\boldsymbol{f}_t$ is the passive tissue forces, $k_p = 2.225 \cdot 10^{-3} \mathrm{Nm/rad}$, $k_c = 34.53 \cdot 10^{-3} \mathrm{Nm/rad}^3$ and $k_v = 2 \cdot 10^{-3} \mathrm{Nm/(rad/s)}$ the physiological constants Robinson et al. (1969); Collins et al. (1981); Priamikov et al. (2016) and $\boldsymbol{q}, \dot{\boldsymbol{q}} \in \Re^3$ the rotational coordinates and velocities of the mode. These forces are modeled using `OpenSim`'s expression based coordinate force.

Results

Fixation Controller

A fixation controller that calculates the EOMs excitations required to track a desired saccade was implemented. The controller actuates the model in a closed-loop Forward Dynamics (FD) manner. The parameters of the controller are the desired horizontal and vertical fixation angles, the saccade onset and velocity, and the gains of Proportional Derivative (PD) tracking controller. A sigmoid function is used for generating smooth saccade trajectories in the horizontal and vertical direction, while the torsional component is maintained close to zero. More formally,

$$\theta_d(t) = \frac{a}{2}\big(\tanh(b(t - t_0)) + 1\big)$$
$$\dot{\theta}_d(t) = \frac{ab}{2}(1 - \tanh^2(b(t - t_0))) \tag{2}$$

where $\theta_d(t)$ and $\dot{\theta}_d(t)$ represent the desired orientation and velocity at time t, a the magnitude of the trajectory, b the slope and t_0 a time shift constant. Provided a fixation goal θ_g, a desired saccade velocity $\dot{\theta}_g$ and a saccade onset t_g, the parameters of the sigmoid function are defined as $a = \theta_g$, $b = 2\dot{\theta}_g/\theta_g$ and $t_0 = t_s$. The output of the PD tracking controller has the following form

$$u(t) = k_p(\theta_d(t) - \theta(t)) + k_d(\dot{\theta}_d(t) - \dot{\theta}(t)) \tag{3}$$

where k_p, k_d are the tracking gains, and $\theta(t)$, $\dot{\theta}(t)$ the simulated response of the model.

The sign and magnitude of $u(t)$, representing the deviation from the fixation target for each axis of rotation respectively, are used to calculate the muscle excitation levels, by assuming that each individual muscle rotates the eye globe in a particular direction. Figure 2 presents an instance of the model during simulation with the corresponding muscles activated. Figure 3 depicts the simulated coordinates, angular velocities and estimated EOMs excitation levels that reproduce the desired saccade trajectory for different model parameters. Finally, Figure 4 shows alternations in the saccadic movements both in the horizontal and vertical direction so as to examine the activation and deactivation patterns of the EOMs.

Conclusion

A realistic oculomotor model representing the motility of a normal human eye was presented and made publicly available. The parameters of the model were calibrated using available experimental measured data. The model can be used for kinematics and dynamics analysis or as a tool for obtaining the muscle activations that generate a desired saccade, using a closed-loop fixation controller in a FD manner. There is of course space for further improvement, which will enhance the accuracy and the predictability of the proposed computational model. In this study, we didn't attempt to model the muscle pulleys Kono et al. (2002), where the position of the pulleys vary as a function of the model coordinates. Therefore, the users should consider performing further validation of the eye model based on the requirements of the targeted utility and the variables of interests.
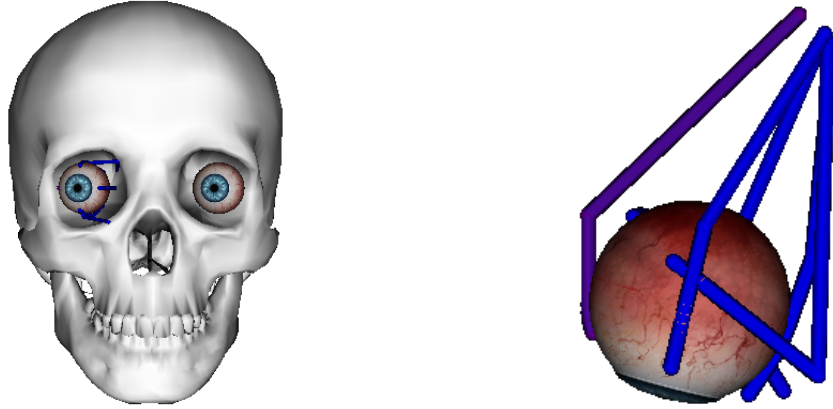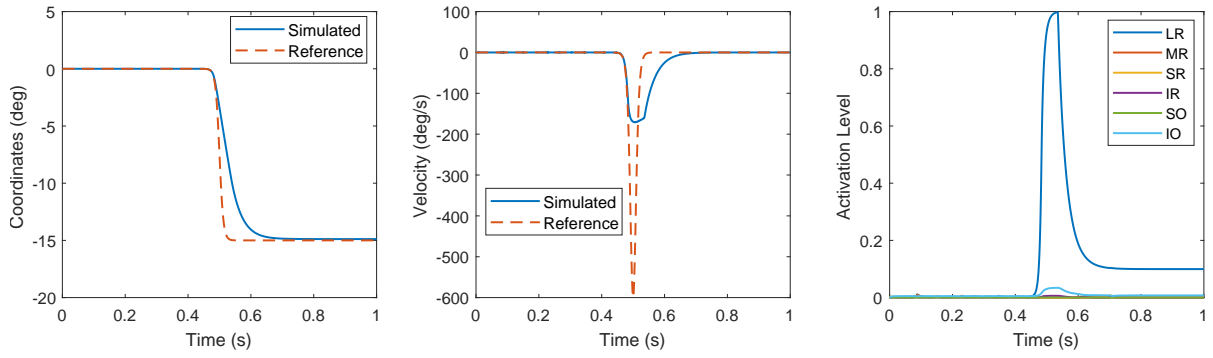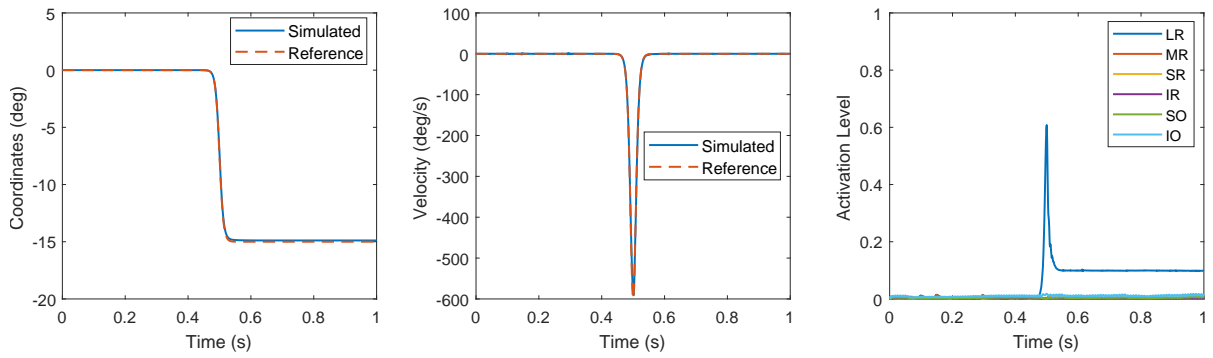
Figure 2: Model with a fixation target at $\theta_H = -15°$, $\theta_V = 0°$ during simulation. Blue denotes low and red high muscle activation levels.

(a) $\theta_H = -15°$, $\theta_V = 0°$, $b = 600°/\mathrm{s}$ and $k_v = 0.002\mathrm{Nm}/(\mathrm{rad}/\mathrm{s})$

(b) $\theta_H = -15°$, $\theta_V = 0°$, $b = 600°/\mathrm{s}$ and $k_v = 0\mathrm{Nm}/(\mathrm{rad}/\mathrm{s})$

Figure 3: Simulated saccade response for different model parameters. Left subplot represents the simulated generalized coordinates, middle the generalized velocities and right the estimated EOMs excitation levels.
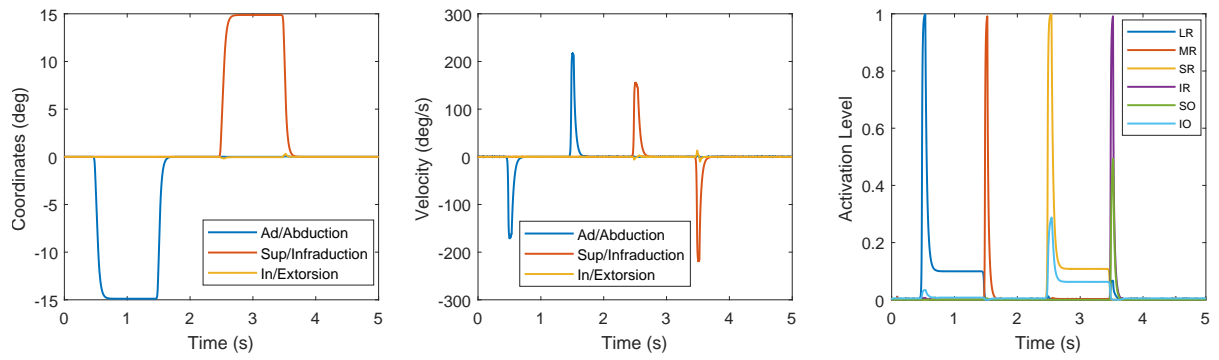
Figure 4: Simulated saccade response performing abduction/adduction $(0 - 2s)$ and supraduction/infraduction $(2 - 4s)$ with $k_v = 0.002 \text{Nm}/(\text{rad}/s)$.

Bibliography

S.-h. Lee and D. Terzopoulos, "Heads Up ! Biomechanical Modeling and Neuromuscular Control of the Neck," *ACM Transactions on Graphics*, vol. 1, no. 212, pp. 1188–1198, 2006.

S. L. Delp, F. C. Anderson, A. S. Arnold, P. L. Loan, A. Habib, C. T. John, E. Guendelman, and D. G. Thelen, "OpenSim : Open-Source Software to Create and Analyze Dynamic Simulations of Movement," *IEEE Transactions on Biomedical Engineering*, vol. 54, no. 11, pp. 1940–1950, 2007.

D. A. Robinson, D. M. O'meara, A. B. Scott, and C. C. Collins, "Mechanical components of human eye movements," *Journal of Applied Physiology*, vol. 26, no. 5, pp. 548–553, 1969.

C. C. Collins, M. R. Carlson, a. B. Scott, and a. Jampolsky, "Extraocular muscle forces in normal human subjects." *Investigative Ophthalmology & Visual Science*, vol. 20, no. 5, pp. 652–664, 1981.

J. Iskander, M. Hossny, S. Nahavandi, L. del Porto, and L. Porto, "An ocular biomechanic model for dynamic simulation of different eye movements," *Journal of Biomechanics*, 2018.

D. A. Robinson, "The mechanics of human saccadic eye movement," *The Journal of Physiology*, pp. 245–264, 1964.

D. A. Robinson and A. F. Fuchs, "Eye movements evoked by stimulation of frontal eye fields." *Journal of Neurophysiology*, vol. 32, no. 5, pp. 637–648, 1969.

D. G. Thelen, F. C. Anderson, and S. L. Delp, "Generating dynamic simulations of movement using computed muscle control," *Journal of Biomechanics*, vol. 36, no. 3, pp. 321–328, mar 2003.

M. Millard, T. Uchida, A. Seth, and S. L. Delp, "Flexing computational muscle: modeling and simulation of musculotendon dynamics," *Journal of Biomechanical Engineering*, vol. 135, no. 2, pp. 1–12, mar 2013.

S. S. James, C. Papapavlou, A. Blenkinsop, A. J. Cope, S. R. Anderson, K. Moustakas, and K. N. Gurney, "Integrating brain and biomechanical models-A new paradigm for understanding neuro-muscular control," *Frontiers in Neuroscience*, vol. 12, no. FEB, 2018.

A. Priamikov, M. Fronius, B. Shi, and J. Triesch, "OpenEyeSim: A biomechanical model for simulation of closed-loop visual perception," *Journal of Vision*, vol. 16, no. 15, p. 25, dec 2016.

R. Kono, R. A. Clark, and J. L. Demer, "Active pulleys: Magnetic resonance imaging of rectus muscle paths in tertiary gazes," *Investigative Ophthalmology and Visual Science*, vol. 43, no. 7, pp. 2179–2188, 2002.

R. A. Clark, J. M. Miller, and J. L. Demer, "Three-dimensional Location of Human Rectus Pulleys by Path Inflections in Secondary Gaze Positions," *Investigative Ophthalmology & Visual Science*, vol. 41, no. 12, pp. 3787–3797, nov 1977.

J. M. Miller, "Understanding and misunderstanding extraocular muscle pulleys," *Journal of Vision*, vol. 7, no. 11, p. 10, 2007.

Q. Wei, S. Sueda, and D. K. Pai, "Physically-based modeling and simulation of extraocular muscles," *Progress in Biophysics and Molecular Biology*, vol. 103, no. 2-3, pp. 273–283, dec 2010.

P. Bach-y Rita, C. C. Collins, Smith-Kettlewell Institute of Visual Sciences., and University of the Pacific. Department of Visual Sciences., *The control of eye movements.* Academic Press, 1971.

D. E. Angelaki and B. J. M. Hess, "Control of eye orientation : where does the brain ' s role end and the muscle ' s begin ?" *Neuroscience*, vol. 19, 2004.

A. M. Wong, "Listing's law: clinical significance and implications for neural control," *Survey of Ophthalmology*, vol. 49, no. 6, pp. 563–575, nov 2004.